# Entorhinal Cortex Layer III Input to the Hippocampus Is Crucial for Temporal Association Memory

Junghyup Suh, *et al.*

*Science* **334**, 1415 (2011);
DOI: 10.1126/science.1210125

The neurofeedback provided to participants was based on activation patterns only in V1/V2. However, this procedure might have induced neural activities in areas other than V1/V2, which might also contribute to VPL. To test whether other regions quantitatively contributed to VPL, we conducted two offline tests with other areas (such as V3, V4, the intraparietal sulcus, and the lateral prefrontal cortex) that have been implicated in VPL (*6*–*8*).

If the orientation-specific activation patterns in V1/V2 during the induction stage induced similar orientation-specific brain activities in other areas, the activation patterns in those areas should predict the target-orientation likelihood in V1/V2 on a trial-by-trial basis. In the first offline test, we employed a sparse linear regression method (*14*) to predict the target-orientation likelihoods in V1/V2 from activation patterns in those higher areas in each trial during the induction stage (SOM). Goodness of prediction for the target-orientation likelihood in V1/V2 by other areas, or prediction accuracies of the sparse linear regression, was evaluated by coefficients of determination, all of which were less than 5% (fig. S9A).

We conducted a second offline test to examine the possibility that the decoder simply performed poorly in higher brain areas. We examined whether accurate orientation information can be read out from each brain area when real orientation stimuli are presented in the decoder construction stage. As was done for V1/V2 during the fMRI decoder construction stage, we built a multinomial sparse logistic regression decoder to classify activation patterns into each of the three orientations (SOM). Decoding accuracies were significantly higher than chance level in all of these areas (fig. S9B, also compare fig. S9, A and B). The results of these two offline tests indicate that influences of the neurofeedback on VPL were largely confined to early visual areas such as V1/V2.

Our results indicate that the adult early visual cortex is so plastic that mere repetition of the activity pattern corresponding to a specific feature in the cortex is sufficient to cause VPL of a specific orientation, even without stimulus presentation, conscious awareness of the meaning of the neural patterns that participants induced, or knowledge of the intention of the experiment. How is the present research on VPL distinguished from previous approaches? Unit recording and brain imaging studies have successfully revealed the correlation between VPL and neural activity changes (*1*–*8*). However, these correlation studies cannot clarify cause-and-effect relationships. The studies that examined the effect of a lesion (*15*) or transcranial magnetic stimulation (TMS) (*16*, *17*) to a brain region on VPL have shown whether the examined region plays some role in VPL. However, these studies cannot clarify how particular activity patterns in the region are related to VPL. In contrast, the present decoded fMRI neurofeedback method allowed us to induce specific neural activity patterns in V1/V2, which caused VPL.

The present decoded fMRI neurofeedback method can be used to clarify cause-and-effect relationships in many functions in system neuroscience (*18*, *19*). Although previous fMRI online-feedback training is a promising technique for influencing human behaviors (*10*–*13*), as in lesion or TMS studies, it could at best reveal influences of the entire extent of an area/region on learning/memory, which is a certain limitation for neuroscientific research (*20*). In contrast, the present decoded fMRI neurofeedback method induces highly selective activity patterns within a brain region, thus allowing the investigator to influence specific functions. It can "incept" a person to acquire new learning, skills, or memory, or possibly to restore skills or knowledge that has been damaged through accident, disease, or aging, without a person's awareness of what is learned or memorized.


**References and Notes**

1. A. Schoups, R. Vogels, N. Qian, G. Orban, *Nature* **412**, 549 (2001).
2. Y. Yotsumoto, T. Watanabe, Y. Sasaki, *Neuron* **57**, 827 (2008).
3. T. Hua *et al*., *Curr. Biol.* **20**, 887 (2010).
4. N. Censor, Y. Bonneh, A. Arieli, D. Sagi, *J. Vision* **9**, 1 (2009).
5. A. Karni, D. Sagi, *Nature* **365**, 250 (1993).
6. C. T. Law, J. I. Gold, *Nat. Neurosci.* **11**, 505 (2008).
7. T. Yang, J. H. Maunsell, *J. Neurosci.* **24**, 1617 (2004).
8. C. M. Lewis, A. Baldassarre, G. Committeri, G. L. Romani, M. Corbetta, *Proc. Natl. Acad. Sci. U.S.A.* **106**, 17558 (2009).
9. O. Yamashita, M. A. Sato, T. Yoshioka, F. Tong, Y. Kamitani, *Neuroimage* **42**, 1414 (2008).
10. S. Bray, S. Shimojo, J. P. O'Doherty, *J. Neurosci.* **27**, 7498 (2007).
11. A. Caria *et al*., *Neuroimage* **35**, 1238 (2007).
12. R. C. deCharms *et al*., *Neuroimage* **21**, 436 (2004).
13. N. Weiskopf *et al*., *Neuroimage* **19**, 577 (2003).
14. A. Toda, H. Imamizu, M. Kawato, M. A. Sato, *Neuroimage* **54**, 892 (2011).
15. K. R. Huxlin *et al*., *J. Neurosci.* **29**, 3981 (2009).
16. E. Corthout, B. Uttl, V. Walsh, M. Hallet, A. Cowey, *Neuroreport* **11**, 1565 (2000).
17. F. Giovannelli *et al*., *Neuropsychologia* **48**, 1807 (2010).
18. H. R. Dinse, P. Ragert, B. Pleger, P. Schwenkreis, M. Tegenthoff, *Science* **301**, 91 (2003).
19. Y. Miyashita, *Science* **306**, 435 (2004).
20. M. Kawato, *Philos. Trans. R. Soc. London Ser. B* **363**, 2201 (2008).



**Acknowledgments:** This work was conducted in "Brain Machine Interface Development" under the Strategic Research Program for Brain Sciences by the Ministry of Education, Culture, Sports, Science and Technology of Japan. T.W. was partially supported by NIH grants R01 AG031941 and R01 EY015980 and Y.S. by grants R01 MH091801 and NSF 0964776. We thank J. Dobres, M. Fukuda, G. Ganesh, H. Imamizu, A. R. Seitz, and K. Tanaka for their comments on a draft of this manuscript and M. Fukuda, Y. Furukawa, S. Hirose, M. Sato, and ATR BAIC for technical assistances.


**Supporting Online Material**

www.sciencemag.org/cgi/content/full/334/6061/1413/DC1
Materials and Methods
Figs. S1 to S9
References (*21*–*31*)


1 August 2011; accepted 26 October 2011
10.1126/science.1212003




# Entorhinal Cortex Layer III Input to the Hippocampus Is Crucial for Temporal Association Memory


**Junghyup Suh,[1] Alexander J. Rivest,[1] Toshiaki Nakashiba,[1] Takashi Tominaga,[2] Susumu Tonegawa[1]***



**Associating temporally discontinuous elements is crucial for the formation of episodic and working memories that depend on the hippocampal-entorhinal network. However, the neural circuits subserving these associations have remained unknown. The layer III inputs of the entorhinal cortex to the hippocampus may contribute to this process. To test this hypothesis, we generated a transgenic mouse in which these inputs are specifically inhibited. The mutant mice displayed significant impairments in spatial working-memory tasks and in the encoding phase of trace fear-conditioning. These results indicate a critical role of the entorhinal cortex layer III inputs to the hippocampus in temporal association memory.**


A critical feature of episodic memory shared by some forms of working memory is the ability to associate temporally discontinuous elements, called temporal association memory (*1*–*3*). However, the neural circuits within the entorhinal cortex (EC)–hippocampus (HP) network subserving this type of association have remained unknown. The EC provides inputs to the HP via two major projections (Fig. 1A): the trisynaptic pathway (TSP) originating from EC layer II and the monosynaptic pathway (MSP) originating from EC layer III (ECIII). Studies on genetically engineered mice (*4*–*7*) and lesioned rats (*8*–*11*) have demonstrated crucial roles of the TSP in several features of episodic-memory processing, such as pattern completion (*5*–*8*) and separation (*4*, *8*). In contrast, the MSP contributions to episodic-memory processing remain poorly known. We tested the


[1]The Picower Institute for Learning and Memory, RIKEN–MIT Center for Neural Circuit Genetics, Department of Biology and Department of Brain and Cognitive Sciences, Massachusetts Institute of Technology, Cambridge, MA 02139, USA. [2]Department of Neurophysiology, Faculty of Pharmaceutical Sciences, Tokushima Bunri University, Kagawa, Japan.

*To whom correspondence should be addressed. E-mail: tonegawa@mit.edu

hypothesis that the MSP is necessary for temporal association memory.

We created a Cre transgenic mouse, pOxr1-Cre (*12*). X-gal staining and thionin staining on brain sections from the progeny of pOxr1-Cre and Rosa26 (lacZ reporter line) crosses revealed that, by 12 weeks of age, Cre-loxP recombination was restricted to superficial layers of the dorsal portion of the medial EC (MEC) and occurred sparsely in the lateral EC (LEC) (Fig. 1, B and C, and figs. S1 and S2). Immunofluorescence studies with anti–β-galactosidase (β-gal, recombination marker) (Fig. 1, D and E, and fig. S3), anti-NeuN (Fig. 1D and figs. S3 and S4), anti-PGP9.5 (fig. S3), and anti-parvalbumin (Fig. 1E and fig. S3) or anti–GAD-67 (fig. S3) indicated that recombination was mostly confined to excitatory neurons in the MEC superficial layers.

To further define the distribution of recombination within the superficial layers, we conducted neuronal tracing experiments using the retrograde tracer AlexaFluor488–cholera toxin subunit B (CTB) injected into hippocampal subregions of the progeny of pOxr1-Cre and Rosa26 crosses. CTB injection into the stratum lacunosum moleculare (SLM) of dorsal CA1 (Fig. 1F) led to colabeling of only dorsal MEC layer III (MECIII)

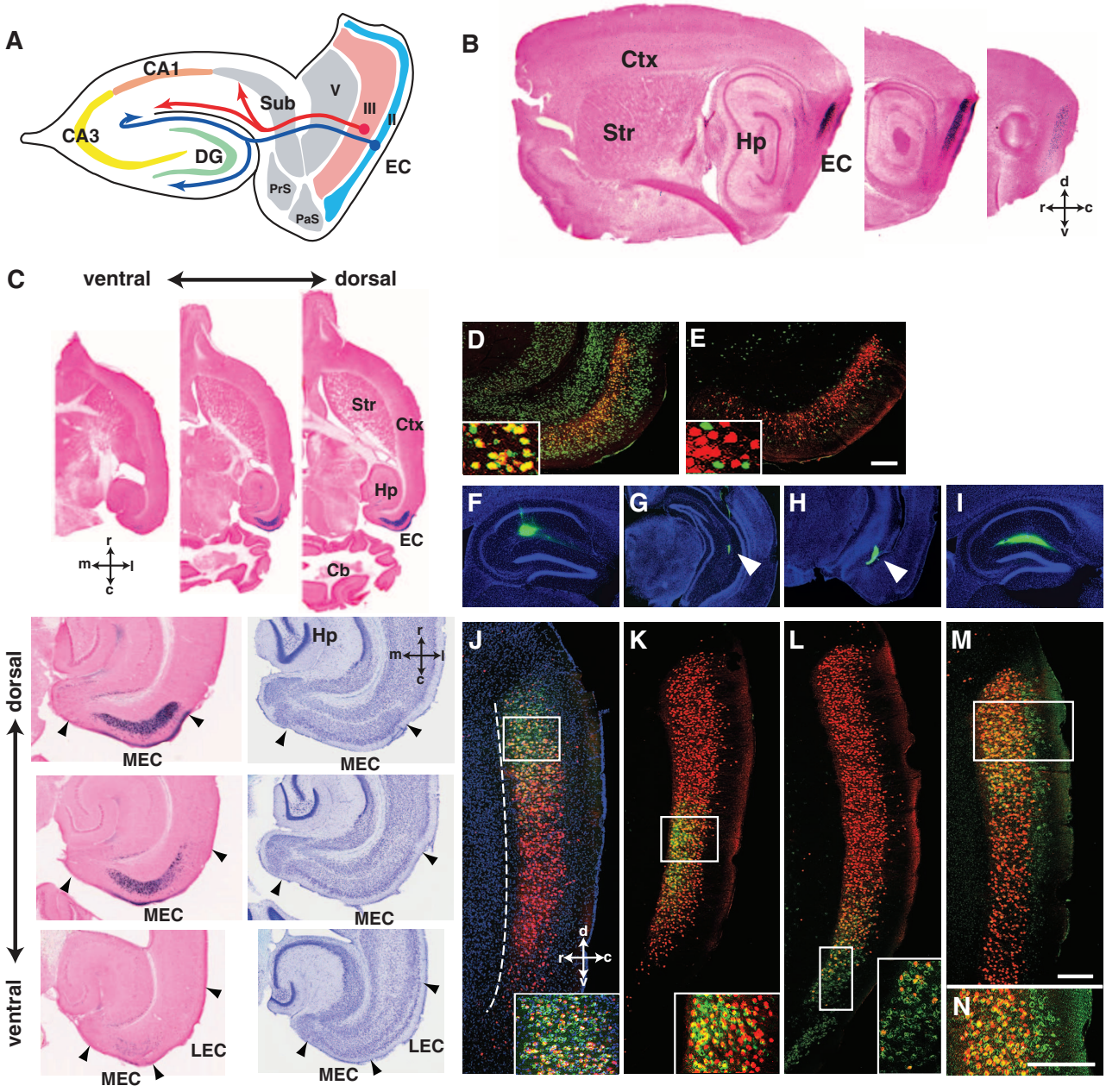


**Fig. 1.** Spatial specificity of Cre-loxP recombination in pOxr1-Cre transgenic mice. (**A**) Schematic of inputs from EC to HP, layer III (red, MSP) to CA1 and subiculum (Sub), and layer II (blue) to CA3 and DG. PrS, presubiculum; PaS, parasubiculum; V, layer V. (**B** and **C**) Parasagittal (B) and horizontal (C) brain sections of 12-week-old pOxr1-Cre/Rosa26 mice stained with X-gal and nuclear fast red. Adjacent sections stained with thionin (C). Arrowheads in (C) indicate MEC and LEC boundaries. Cb, cerebellum; Ctx, cortex; Str, striatum; r, rostral; c, caudal; l, lateral; m, medial. (**D** and **E**) Double immunofluorescence staining of horizontal sections of pOxr1-Cre/Rosa26 mouse with anti–β-gal [(D) and (E), red] and anti-NeuN [(D), green] or anti-parvalbumin [(E), green]. Colabeled cells in (D) are shown in yellow. (**F** to **I**) Injection sites of retrograde tracer, CTB (green), in the SLM of dorsal CA1 (F), intermediate CA1 (G), ventral CA1 (H), and the hippocampal fissure of dorsal CA1 (I). Arrowheads in (G) and (H) indicate the injection sites. (**J** to **M**) Parasagittal sections visualized with CTB-labeled cell body (green) and immunostained by anti–β-gal (red) in the EC. The dotted line denotes the lamina dissecans (J). (**N**) Magnified image from (M). Scale bars, 100 μm.

(Fig. 1J) by CTB and β-gal, whereas the injection of CTB into intermediate CA1 SLM (Fig. 1G) resulted in colabeling restricted to intermediate MECIII (Fig. 1K). In contrast, injection of the tracer into ventral CA1 SLM (Fig. 1H) led to labeling of ventral MECIII, which was poorly colabeled with β-gal (Fig. 1L). When CTB was injected into the hippocampal fissure, which covers both CA1 SLM (receives ECIII projections) and dentate gyrus (DG) stratum moleculare (receives ECII projections) (Fig. 1I) (*13*), we observed colabeling in the dorsal MECIII (Fig. 1, M and N). More importantly, there was a clear segregation of the layer II and layer III cells, confirming that recombination was primarily restricted to the MECIII (Fig. 1N and fig. S4).

To selectively inhibit synaptic transmission at the MECIII to CA1/subiculum synapses by use of the tetanus toxin light chain (TeTX), we crossed the pOxr1-Cre mouse (Tg1) with the pαCaMKII-loxP-STOP-loxP-tTA mouse (Tg2) and the tetO-TeTX mouse (Tg3) (Fig. 2A) (*5*). To examine the input-output relationship of transmission at the ECIII-CA1 synapses, we employed the fluorescent voltage-sensitive dye (VSD) imaging method (Fig. 2B and fig. S5) (*14*) on hippocampal slices prepared from the triple-transgenic mutant, MECIII-TeTX, and control mice (Tg1 x Tg2), which were raised on a doxycycline (Dox)–containing diet followed by 4 to 8 weeks of a Dox-free diet (Fig. 2, C and F). The MECIII-TeTX mice showed a significant reduction (78.4 to 95.9%) in postsynaptic fluorescence with SLM stimulation compared with controls (Fig. 2, B and D), whereas no difference of fluorescence was observed between the genotypes with stratum radiatum (SR) stimulation (Fig. 2, B and E). When hippocampal slices were prepared from MECIII-TeTX mice off Dox for 4 weeks, the postsynaptic fluorescence was reduced and matched that of the slices from MECIII-TeTX mice off Dox for 8 weeks (Fig. 2F and fig. S6). With 4 weeks of Dox withdrawal followed by 4 weeks of Dox readministration, the postsynaptic fluorescence at ECIII-CA1 synapses was restored in MECIII-TeTX mice to levels comparable to controls (Fig. 2F and fig. S6). These results demonstrate that transmission in MECIII-TeTX mice can be inhibited specifically at the MECIII-CA1 synapses in an inducible and reversible manner. Combined with the CTB tracing data from the pOxr1-Cre/Rosa26 mouse (Fig. 1, F to N), we conclude that inhibition of neuronal transmission in the MECIII-TeTX mice was restricted to synapses of the projections from the dorsal and intermediate MECIII neurons to the HP. The MECIII-TeTX mice raised on a Dox diet followed by 4-weeks of Dox withdrawal will be referred to as mutants hereafter, unless indicated otherwise.

Immunohistological analyses revealed no obvious indications of molecular and cytoarchitectural abnormalities in the EC (figs. S7, S8, and S10) and HP (figs. S7 to S9). The mutants displayed no detectable abnormalities in anxiety, motor coordination, or pain sensitivity (fig. S11). The mutants were also normal in the acquisition, recall, and consolidation of spatial reference memory (figs. S12 and S13) and in the basic properties of place fields of CA1 pyramidal neurons and interneurons (fig. S14) (*15*).

The mutants exhibited a deficit in a water-maze version of the delayed matching-to-place (DMP) task (Fig. 3A) designed to test spatial working memory, a form of temporal association memory. During early training (block 0 to block 2), the mutants showed normal escape latencies compared to controls (Fig. 3B), presumably because they were still learning the task requirements and rules (*16*, *17*). As training advanced and the platform size was reduced (blocks 3 and 4), however, the mutants' escape latencies became greater compared with the controls in runs 2 to 4. Consequently, the savings (escape latency difference between runs 1 and 2) were less for the mutants in block 3 ($t = 2.564$, $P < 0.05$) and block 4 ($t = 4.132$, $P < 0.001$) (Fig. 3C), indicating an impairment in spatial working memory.

We next subjected both genotypes to a delayed non–matching-to-place (DNMP) version of the T-maze task (Fig. 3D). The controls showed a significant improvement in performance between day 1 and day 12 (fig. S15). In contrast, the mutants were impaired in this task over the 12-day period (10 trials per day) [two-way analysis of

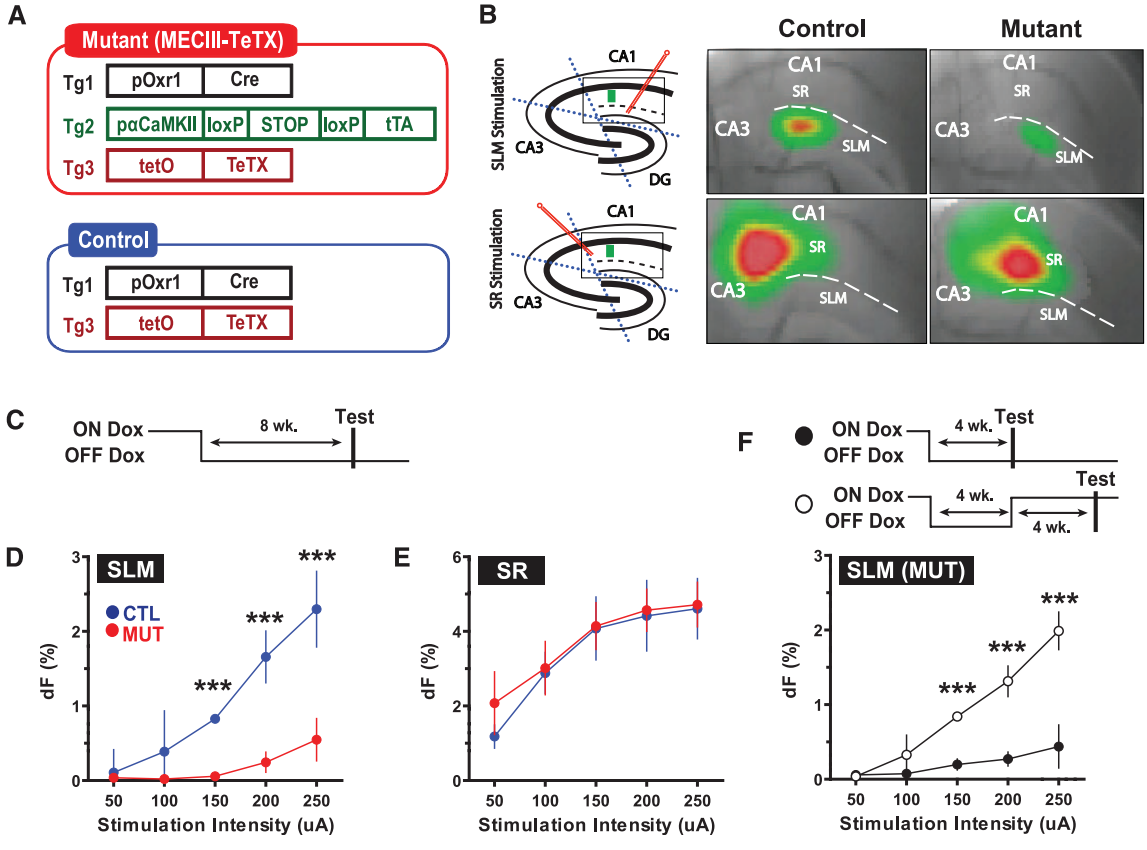


**Fig. 2.** Triple-transgenic MECIII-TeTX mouse (mutant) and inducible and reversible inhibition of MECIII input to CA1. (**A**) Breeding strategies for mutant and control mice. (**B**) VSD imaging of transverse hippocampal sections. A stimulating electrode (red bar) was placed in SLM or SR, and fluorescent signal was measured in SR (green square). Dotted black lines indicate knife cuts to separate CA3 and DG from CA1. Fluorescent signal changes are displayed in pseudocolor after SLM or SR stimulation in control and mutant slices. Dashed white lines indicate the boundary between SR and SLM. (**C**) Dox withdrawal schedule in VSD experiments for (D) and (E). (**D** and **E**) Input-output relationships after SLM or SR stimulation in mutant and control slices. dF, fractional changes in fluorescence. (**F**) Reversibility of the synaptic inhibition. VSD imaging was performed 4 weeks after Dox withdrawal (solid circles) and after 4 weeks of Dox withdrawal followed by 4 weeks of Dox readministration (empty circles) in mutant slices after SLM stimulation. Asterisks indicate the significance at the 0.001 level; error bars indicate SEMs.

variance: genotype, $F_{1,360} = 96.75$, $P < 0.0001$] (Fig. 3, E and F) and did not display an improvement (fig. S15), confirming the mutants' impairment in spatial working memory.

To investigate whether the MECIII input to the HP plays a role in nonspatial temporal association, we subjected the mutant and control mice to trace fear-conditioning (TFC). In this task, a tone [conditioned stimulus (CS)] must be associated with a footshock [unconditioned stimulus (US)] delivered subsequently with a 20-s time gap. The mutants froze less than controls during the training composed of three CS-US pairs (Fig. 4A). The next day, in a distinct novel chamber, mutants froze less than controls in response to tone presentation (Fig. 4A). Conversely, when the temporal gaps between the CS and US were eliminated [delay fear-conditioning (DFC)], there were no freezing differences between the two genotypes during either the acquisition or the recall phase (Fig. 4B). To investigate whether the MSP is required during the acquisition and/or recall phase in TFC, we targeted the inhibition of synaptic transmission to each of these two phases. When inhibition was targeted to the acquisition phase, mutants froze less than controls in response to tone (Fig. 4C), whereas when inhibition was targeted to the recall phase, we observed no freezing difference between the genotypes (Fig. 4D).

To further investigate the role of the EC-HP circuits in temporal association memory, we examined whether the indirect ECII input to CA1 via the TSP also played a role in TFC by using a second mutant, the CA3-TeTX mouse (*5*). These mice, in which CA3 input to CA1 is inhibited under Dox withdrawal (*5*), performed similar to controls in the TFC task (Fig. 4E).

We hypothesized that the essential function of the MECIII input to the HP in TFC may be associated with the persistent activity observed in vitro in their cells (*18*, *19*). As this activity depends on activation of the metabotropic glutamate receptor 1 (*19*) and/or cholinergic muscarinic receptors (*20*), we injected a mixture of their respective antago-

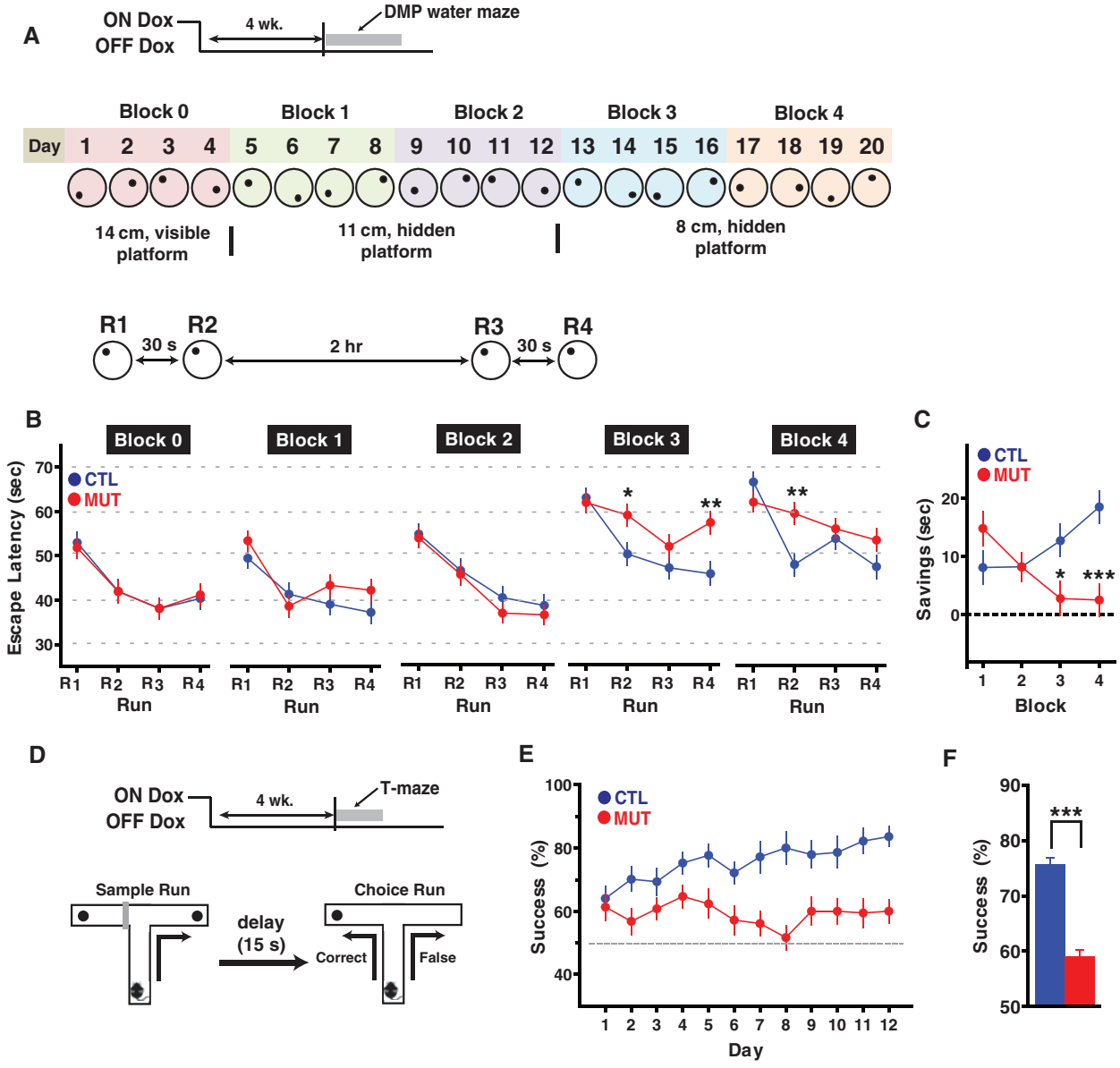


**Fig. 3.** Impairment of MECIII-TeTX mice in the DMP and DNMP tasks. (**A**) Protocol and Dox-schedule for a water-maze version of the DMP task. (**B**) Averaged escape latencies for run 1 (R1), R2, R3, and R4 for each 4-day block. (**C**) Averaged savings. Asterisks in (B) and (C) represent run-specific significance. (**D**) T-maze version of the DNMP task. Black dots represent rewards. (**E**) Success rate on 10 trials each day for 12 days. The gray dashed line denotes the success rate expected by a random arm selection on a choice run (50%). (**F**) Success rates averaged over 12 days. Asterisks indicate the significance at the level of 0.05 or less; error bars indicate SEMs.

nists (LY367385 and scopolamine) or the vehicle bilaterally into the dorsal EC and subjected these mice to TFC. In response to tone, the freezing level of antagonist-injected control mice was less than vehicle-injected control mice, but was not different from antagonist-injected mutants (Fig. 4F). With the same pharmacological treatment, we observed no freezing difference to tone between the genotypes in the DFC task (fig. S16)

In this study, we created a transgenic mouse line in which the synaptic output of the excitatory MEC layer III cells is specifically and reversibly inhibited. Our genetic manipulation and behavior data provided insights into the specific role of MEC layer III projection in the processing of hippocampal-dependent memory.

First, the MECIII input to the HP, an essential component of the MSP, is crucial for temporal associations in spatial working memory. The DMP task required animals to update the association between the platform location and spatial cues daily on the first run and maintain that association for subsequent runs that same day. The DNMP task required animals to associate the sample arm and the alternative reward arm across a delay period. Both of these tasks require a temporal association memory with a temporal gap of 15 to 30 s. Although it is possible that the deficits observed in the mutants are due to their inability to encode spatial/contextual information, this is unlikely because these animals were normal in other spatial/contextual memory tasks (figs. S12 to 14 and S17). Second, a blockade of the MECIII input into the HP resulted in an impairment in TFC, specifically during day 1 when the animals needed to associate the CS and US delivered with an intervening 20-s gap. Again, it is unlikely that the deficits are due to an inability to encode the CS or US because the same mutants were normal in DFC and even in a TFC task with a 40-s trace that may not be hippocampal-dependent (fig. S18) (*21*). Third, our demonstration that the alternative and indirect input to CA1 mediated by the TSP is dispensable for TFC highlights the importance of the MSP in temporal association memory.

In addition to the major projections to CA1/subiculum, MECIII neurons send axons to other EC cells (*22*). We expect that these connections

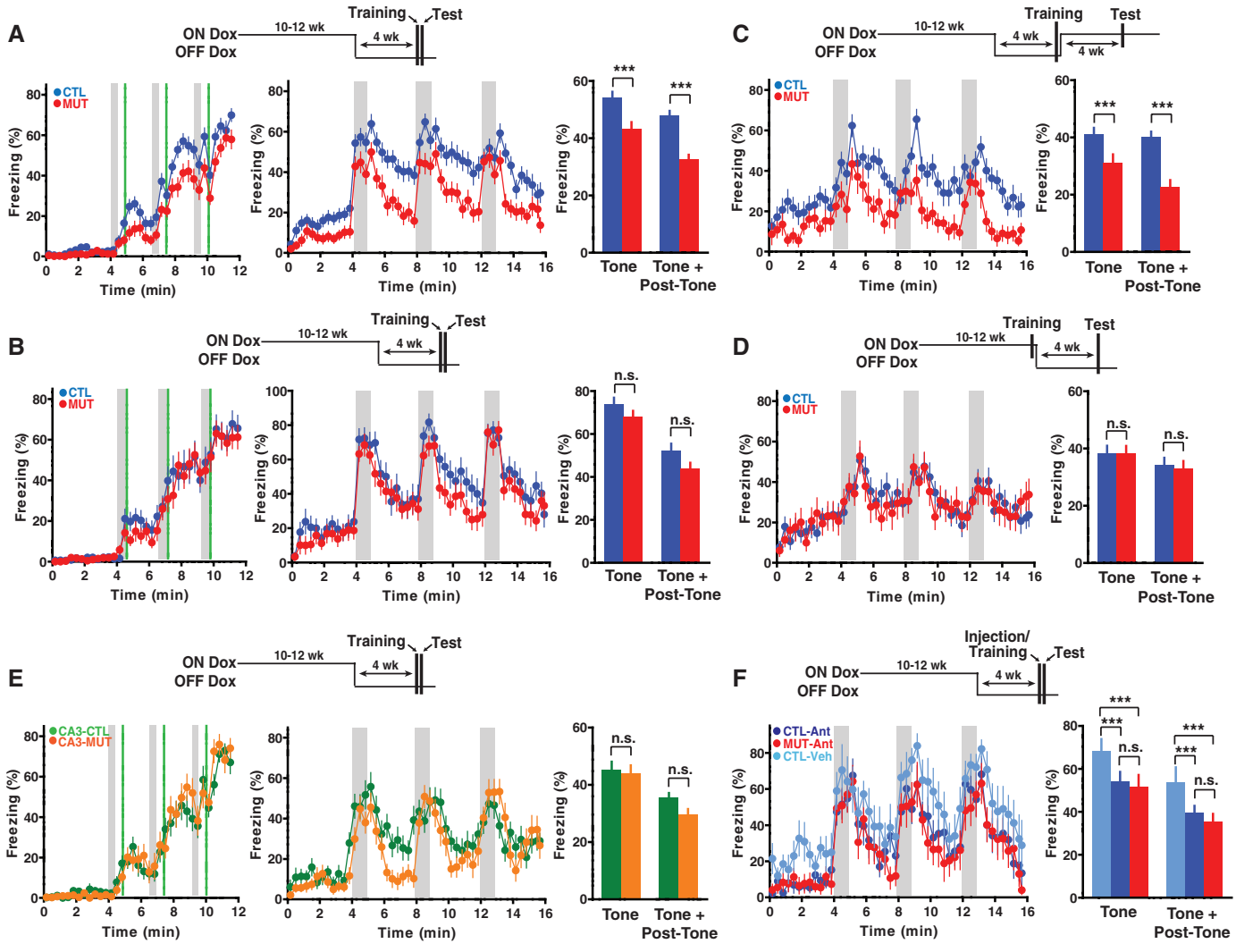


**Fig. 4.** Fear conditionings with two mutants, MECIII-TeTX and CA3-TeTX, and pharmacologically treated mice. (**A** and **B**) Time course of freezing observed in MECIII-TeTX mice in the TFC (A) or DFC task (B) during training on day 1 (left) and testing on day 2 (middle). Gray and green bars represent tone and shock, respectively. Freezing levels during the testing were averaged over three epochs of the 60-s tone period and of the entire 240-s tone plus post-tone periods (right). (**C** and **D**) Time course of freezing (left) and averaged freezing levels (right) of MECIII-TeTX mice during testing of the TFC task in which the synaptic inhibition was targeted to the training (C) or testing (D). (**E**) Time course of freezing of CA3-TeTX mice during the training (left) and testing (middle) of the TFC task. (**F**) Time course of freezing (left) and averaged freezing levels (right) during testing for controls and mutants in the TFC task. Mice were bilaterally injected with either an antagonist mixture or vehicle into dorsal MEC before the training. Asterisks indicate the significance at the level of 0.05 or less; error bars indicate SEMs. n.s., not significant.

are also blocked in the mutants and therefore cannot exclude the possibility that an impairment of intrinsic ECIII circuits contributed to the observed behavioral deficits. However, such an impairment alone can not explain the observed deficits in the hippocampal-dependent memory tasks unless it is translated into an MSP impairment. Thus, a more attractive possibility would be that the lack of transmission of persistent activity from the MECIII (*19*) to CA1/subiculum via the MSP resulted in the behavioral deficits in these hippocampal-dependent tasks, although such activity has yet to be demonstrated in vivo in the mouse. We hypothesize that tone induces sustained activity in the MECIII after its cessation. This persistent activity, perhaps with the help of theta and/or gamma frequency coupling between the MECIII and CA1 (and/or subiculum) (*23*, *24*), may allow the delivery of the CS to the amygdala through CA1 (and/or subiculum) in a manner coincidental with the US signal. The differential effects of the mGluR1 and cholinergic muscarinic receptor antagonists injected into MEC on the TFC and DFC tasks (Fig. 4F and fig. S16) support this hypothesis.

Apart from specific mechanisms, our overall results demonstrate a crucial role of the EC layer III input to the HP in hippocampal-dependent temporal association memory.

### References and Notes


1. M. E. Hasselmo, C. E. Stern, *Trends Cogn. Sci.* **10**, 487 (2006).
2. A. Baddeley, *Nat. Rev. Neurosci.* **4**, 829 (2003).
3. N. S. Clayton, T. J. Bussey, A. Dickinson, *Nat. Rev. Neurosci.* **4**, 685 (2003).
4. T. J. McHugh *et al.*, *Science* **317**, 94 (2007).
5. T. Nakashiba, J. Z. Young, T. J. McHugh, D. L. Buhl, S. Tonegawa, *Science* **319**, 1260 (2008).
6. K. Nakazawa *et al.*, *Science* **297**, 211 (2002).
7. K. Nakazawa, T. J. McHugh, M. A. Wilson, S. Tonegawa, *Nat. Rev. Neurosci.* **5**, 361 (2004).
8. R. P. Kesner, P. E. Gilbert, G. V. Wallenstein, *Curr. Opin. Neurobiol.* **10**, 260 (2000).
9. D. G. Mumby, *Behav. Brain Res.* **127**, 159 (2001).
10. H. A. Steffenach, M. Witter, M. B. Moser, E. I. Moser, *Neuron* **45**, 301 (2005).
11. V. H. Brun *et al.*, *Science* **296**, 2243 (2002).
12. Materials and methods are available as supporting material on *Science* Online.
13. M. P. Witter, D. G. Amaral, in *The Rat Nervous System*, G. Paxinos, Ed. (Elsevier Academic Press, New York, 2004), pp. 635–704.
14. T. Tominaga, Y. Tominaga, H. Yamada, G. Matsumoto, M. Ichikawa, *J. Neurosci. Methods* **102**, 11 (2000).
15. Relevant discussion regarding data in figs. S12 and S14 can be found in the supporting online material.
16. K. Nakazawa *et al.*, *Neuron* **38**, 305 (2003).
17. R. J. Steele, R. G. Morris, *Hippocampus* **9**, 118 (1999).
18. A. V. Egorov, B. N. Hamam, E. Fransén, M. E. Hasselmo, A. A. Alonso, *Nature* **420**, 173 (2002).
19. M. Yoshida, E. Fransén, M. E. Hasselmo, *Eur. J. Neurosci.* **28**, 1116 (2008).
20. F. Esclassan, E. Coutureau, G. Di Scala, A. R. Marchand, *J. Neurosci.* **29**, 8087 (2009).
21. I. Misane *et al.*, *Hippocampus* **15**, 418 (2005).
22. C. B. Canto, F. G. Wouterlood, M. P. Witter, *Neural Plast.* **2008**, 1 (2008).
23. K. Mizuseki, A. Sirota, E. Pastalkova, G. Buzsáki, *Neuron* **64**, 267 (2009).
24. L. L. Colgin *et al.*, *Nature* **462**, 353 (2009).


**Acknowledgments:** We thank C. Ragion, C. Twiss, M. Pfau, M. Ragion, C. Carr, and S. Perry for technical help; N. Arzoumanian for help with manuscript preparation; and D. Buh, J. Young, and other members of the Tonegawa lab for discussion. This work was supported by NIH grants R01-MH078821 and P50-MH58880 (to S.T.) and the RIKEN Brain Science Institute.

### Supporting Online Material

www.sciencemag.org/cgi/content/full/science.1210125/DC1
Materials and Methods
SOM Text
Figs. S1 to S18
References

21 June 2011; accepted 20 October 2011
Published online 3 November 2011;
10.1126/science.1210125

# Interconversion Between Intestinal Stem Cell Populations in Distinct Niches

**Norifumi Takeda,[1,2,3]* Rajan Jain,[1,2,3]* Matthew R. LeBoeuf,[1,4] Qiaohong Wang,[1,2,3] Min Min Lu,[2] Jonathan A. Epstein[1,2,3]†**

**Intestinal epithelial stem cell identity and location have been the subject of substantial research. Cells in the +4 niche are slow-cycling and label-retaining, whereas a different stem cell niche located at the crypt base is occupied by crypt base columnar (CBC) cells. CBCs are distinct from +4 cells, and the relationship between them is unknown, though both give rise to all intestinal epithelial lineages. We demonstrate that *Hopx*, an atypical homeobox protein, is a specific marker of +4 cells. *Hopx*-expressing cells give rise to CBCs and all mature intestinal epithelial lineages. Conversely, CBCs can give rise to +4 *Hopx*-positive cells. These findings demonstrate a bidirectional lineage relationship between active and quiescent stem cells in their niches.**

The multicellular epithelium of the intestine is replaced every few days, and this renewal process is maintained by multipotent intestinal stem cells (ISCs) (*1*, *2*). The location and identity of ISCs have been a subject of much research and debate, with implications for understanding gastrointestinal cancer, repair after intestinal injury, and normal physiology. Numerous reports have suggested that ISCs are located at the +4 position relative to the crypt base (*3*, *4*), while a separate body of work has identified a distinct stem cell niche at the crypt base where crypt base columnar (CBC) cells are interspersed between Paneth cells (*5*–*7*). The +4 cells correspond to the location of slow-cycling, label-retaining cells (LRCs) (*3*, *8*) and colocalize with *Bmi1*-expressing cells (*4*), as well as those expressing an *mTert* transgene (*9*, *10*). CBC stem cells, by contrast, are marked by *Lgr5* (*5*). Although +4 cells and CBCs are clearly distinct, lineage-tracing studies have shown that both can give rise to all the various cell types comprising the small intestine epithelium: goblet cells, neuroendocrine cells, Paneth cells, and epithelial absorptive cells. However, the relationship between these two distinct stem cell populations remains incompletely understood. A recent report suggests that +4 cells can compensate for the loss of CBCs to maintain homeostasis after experimental ablation of *Lgr5*-expressing cells (*11*). However, a bidirectional lineage relationship between active and quiescent populations of stem cells in multiple tissues has also been postulated (*2*), though experimental evidence to support this proposal has been lacking. Here, we show that quiescent +4 ISCs express the atypical homeobox gene *Hopx* and give rise to *Lgr5*-expressing CBCs. Conversely, rapidly cycling CBCs expressing *Lgr5* give rise to +4 cells expressing *Hopx*. These findings reconcile controversies regarding the location and identity of ISCs and demonstrate interconversion between organ-specific stem cell niches.

*Hopx* encodes an atypical homeodomain-containing protein that has previously been studied in the heart and neural stem cells (*12*–*14*). Analysis of the intestines of *Hopx lacZ* knock-in ($Hopx^{LacZ/+}$) mice revealed robust expression of β-galactosidase (β-Gal) in intestinal crypts along the entire length of the intestine (Fig. 1A and fig. S1A). Expression was strongest in the +4 region and included label-retaining cells identified after irradiation and pulse labeling with 5-bromodeoxyuridine (BrdU) (*9*, *15*, *16*) (Fig. 1B and fig. S1B). Eighty-six percent (68/79) of non-Paneth BrdU-retaining cells expressed β-Gal, and nearly all were at or near the +4 position

[1]Department of Cell and Developmental Biology, Perelman School of Medicine at the University of Pennsylvania, Philadelphia, PA 19104, USA. [2]Penn Cardiovascular Institute, Perelman School of Medicine at the University of Pennsylvania, Philadelphia, PA 19104, USA. [3]Institute of Regenerative Medicine, Perelman School of Medicine at the University of Pennsylvania, Philadelphia, PA 19104, USA. [4]Department of Dermatology, Perelman School of Medicine at the University of Pennsylvania, Philadelphia, PA 19104, USA.

*These authors contributed equally to this work.
†To whom correspondence should be addressed. E-mail: epsteinj@mail.med.upenn.edu